TOPOGRAPHIC MAPPING CAPABILITY ANALYSIS OF MARS EXPLORATION ROVER 2003 MISSION IMAGERY

K. Di, R. Li

Mapping and GIS Laboratory, Dept. of Civil & Env. Eng. & Geodetic Science, The Ohio State University
470 Hitchcock Hall, 2070 Neil Ave., Columbus, OH 43210-1275 USA - (di.2, li.282)@osu.edu

Commissions I and V, IC WG I/V

KEY WORDS: Mars rover, topographic mapping, accuracy, bundle adjustment, wide baseline

ABSTRACT:

This paper presents a comprehensive analysis of the topographic mapping capabilities of images from the Mars Exploration Rover 2003 (MER) mission. The 3D measurement accuracies of Pancam (panoramic camera) and Navcam (navigation camera) stereo pairs are estimated using basic photogrammetric principles. The mapping capabilities of single-site panoramas, multi-site panoramas, and wide-baseline stereo images are analyzed based on the bundle adjustment technology. This analysis provides an overview of understanding the attainable geometric accuracies from the images and for best usage of the resultant mapping products during and after the MER mission.

1. INTRODUCTION

During the 2003 Mars Exploration Rover (MER) mission, the identical Spirit and Opportunity rovers landed on January 4 and January 25, respectively. As of February, 2007, they had been exploring their Gusev Crater (Spirit) and Meridiani Planum (Opportunity) landing sites for more than three years using identical science and engineering instrument payloads as shown in Figure 1 (Squyres et al., 2003, 2004; Arvidson et al., 2004). High accuracy in localization of the rovers and in mapping of the surrounding areas are of fundamental importance both for safe rover navigation and for achievement of scientific and engineering goals (Arvidson et al., 2004; Li at al., 2004, 2005). Among the payload instruments, Navcam (navigation camera) and Pancam (panoramic camera) are the ones most important for topographic mapping and rover localization. Navcam is an engineering stereo camera used for navigation purposes (Maki et al., 2003); it has two cameras mounted on the same camera bar of the rover mast as Pancam (see Figure 1). This bar can be rotated 360° in azimuth and ±90° in elevation, enabling the acquisition of full as well as partial panoramas. Pancam is a high-resolution, color stereo panoramic imager used for scientific investigation of the morphology, topography, geology etc, of the two landing sites (Bell et al., 2003). Each of its cameras (left and right) has eight multispectral channels with a 400-1100 nm wavelength range. Since Pancam has a wider stereo base and a longer focal length, it is more effective in mapping medium-to-far objects. The Navcam and Pancam effective depths-of-field are 0.5m-to-infinity and 3m-to-infinity, respectively; their geometric parameters are listed in Table 1.

	Navcam	Pancam
Stereo Base	20 cm	30 cm
Focal Length	14.67 mm	43 mm
Image Dimension	1024 × 1024 pixels	1024 × 1024 pixels
Pixel Size	12 μm	12 μm
Field of View	45° × 45°	16.8° × 16.8°

Table 1. Parameters of the MER Navcam and Pancam cameras

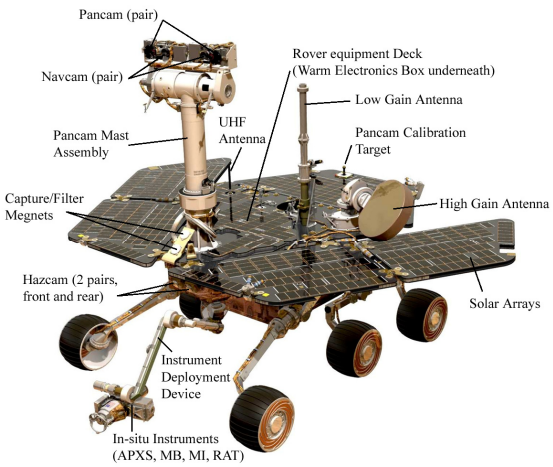

Figure 1. Illustration of the MER rover with its science and engineering payload instruments

One of the important methods used for rover localization and topographic mapping is based on the bundle adjustment of an image network formed by Navcam and Pancam stereo images along the traverse. The overall technology is described in Li et al. (2004) with some technical details explained in papers by team members (Di and Li, 2004; Di et al., 2005; Xu, 2004; Xu et al., 2005). During the MER mission surface operations, The Ohio State University (OSU) team, in collaboration with the Jet Propulsion Laboratory (JPL) and other involved institutions, has been routinely producing topographic maps, rover traverse maps, and updated rover locations from rover images to support both tactical and strategic operations. This information has been provided by OSU through a web-based GIS and has been used for traverse planning and in various scientific investigations by mission scientists (Squyres et al., 2004; Arvidson et al., 2004). The initial mapping and rover localization results have been reported previously in Li et al. (2005, 2006) and Di et al. (2005).

In order to understand the attainable accuracies of the mapping products and their most efficient usage during and after the mission, it is desirable to perform a detailed quantitative analysis of the topographic mapping capabilities of the MER Pancam and Navcam images. This analysis is also important for research on the integration of ground and orbital imagery at the MER landing sites, which will be critical for the advancement of the Mars mapping and rover localization technology. Therefore, this paper presents a comprehensive analysis of the MER Pancam and Navcam topographic mapping capabilities in a systematic way: from stereo pairs to a single panorama, then to multiple panoramas along the rover traverse, and finally to wide-baseline images.

2. EXPECTED 3D MEASUREMENT ACCURACY OF NAVCAM AND PANCAM STEREO PAIRS

Ranging errors of the Navcam and Pancam cameras were briefly discussed in Maki et al. (2003), where a 0.25 pixel correlation error was assumed. Here we give a detailed analysis of their 3D measurement accuracy both as to measurement error in the three directions as well as location of the object in the image.

The "normal case" is a configuration of stereo cameras in which the two camera axes are parallel to each other and perpendicular to the baseline (Figure 2). Navcam has a 0.15° toe-in while Pancam has a 1° toe-in. They are both very close to the "normal case". In addition to the original rover images, linearized images are provided to facilitate stereo image matching. The linearized stereo images are resampled according to epipolar geometry and the toe-in angles have also been eliminated (Alexander et al., 2006). Thus, linearized Navcam and Pancam images, which we use for mapping and localization during mission operations, are "normal case" images. Since the linearization process is based on accurate camera calibration results, the linearized images have the same mapping capabilities (difference is neglectable) as that of the original images. Therefore, it is appropriate to use the "normal case" configuration for analyzing the measurement accuracies of Navcam and Pancam images whether or not they are linearized.

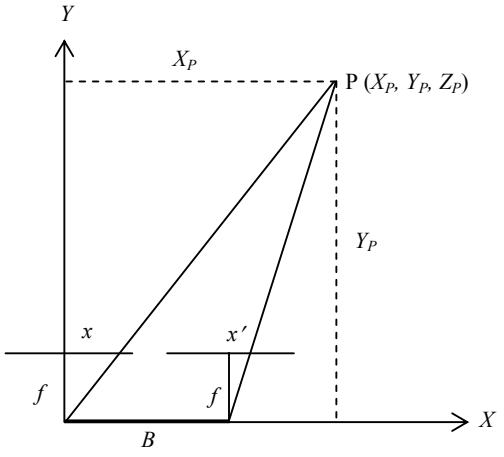

Figure 2. Configuration of the "normal case" stereo pair

In the "normal case" stereo image configuration, the 3D coordinates of an object point $P(X_P, Y_P, Z_P)$ can be calculated using the following parallax equations:

$$X_P = \frac{B}{p}x = \frac{Y_P}{f}x,\ Y_P = \frac{B}{p}f,\ \text{and}\ Z_P = \frac{B}{p}y = \frac{Y_P}{f}y \quad (1)$$

where f is the focal length, B is the base line and p is the parallax, i.e., $p = x - x'$ (see Figure 2). Through error propagation, the accuracies (standard errors σ_X, σ_Y, σ_Z) of the coordinates can be calculated as follows (Wang, 1990):

$$\sigma_Y = \frac{Y_P^{\,2}}{Bf}\sigma_p \quad (2a)$$

$$\sigma_X = \sqrt{\left(\frac{Y_P^{\,2}}{Bf}\right)^2\left(\frac{x}{f}\right)^2\sigma_p^2 + \left(\frac{Y_P}{f}\right)^2\sigma_x^2} \quad (2b)$$

$$\sigma_Z = \sqrt{\left(\frac{Y_P^{\,2}}{Bf}\right)^2\left(\frac{y}{f}\right)^2\sigma_p^2 + \left(\frac{Y_P}{f}\right)^2\sigma_y^2} \quad (2c)$$

where σ_p is the measurement error of parallax (i.e., correlation/matching error) and σ_x and σ_y are the measurement errors of the image coordinates in the horizontal and vertical directions, respectively. It is obvious that the range error (σ_Y) is proportional to the square of the range (Y_P) and that the measurement errors in X and Z are dependent to not only the range, but also the position of the object in the image. At a given range, the minimum error of X lies on the vertical line passing through the image center (where $x = 0$), while the maximum errors of X lie on the left and right margins of the image. Similarly, at a given range, the minimum error of Z lies on the horizontal line passing through the image center (where $y = 0$), while the maximum errors of Z lie on the top and bottom margins of the image. It is interesting to note that the minimum errors in X and Z ($\min\sigma_x = \frac{Y_P}{f}\sigma_x$ and $\min\sigma_y = \frac{Y_P}{f}\sigma_y$) are the same as the ground resolution if we set $\sigma_x = \sigma_y = 1$ pixel.

The parallax measurement accuracy is determined by the accuracy of image matching. According to a theoretical analysis, pixel-level image matching (correlation) has an accuracy of about 1/3 pixel (Zhang and Zhang, 1997), while least-squares matching has an even higher accuracy. Given σ_p = 1/3 pixel, and $\sigma_x = \sigma_y = 1$ pixel, we calculate the standard errors at different ranges for Navcam and Pancam. Figure 3 and Figure 4 show the expected 3D measurement errors of Navcam and Pancam stereo pairs, respectively. Note that the minimum values of σ_X and σ_Z are the same at the same range, as are the maximum values of σ_X and σ_Z. From these figures, we can observe that the range (Y) error is always larger than that in the other two directions and is more severely affected by the distance from the object to the camera. Since range error is the dominant error, we use range error to discuss the general measurement error in the following text if the error is not explicitly specified as being in the X, Y, or Z direction. These figures indicate that the expected measurement error is

reasonable (< 2m) within a range of 38m for Navcam and 80m for Pancam, and that it is less than 1m within a range of 27m for Navcam and 55m for Pancam,.

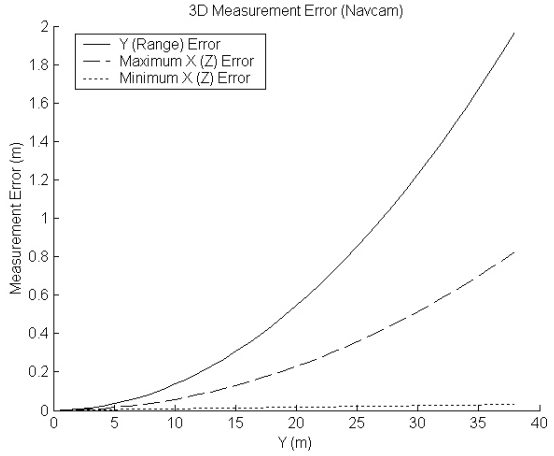

Figure 3. Expected 3D measurement errors for a Navcam stereo pair

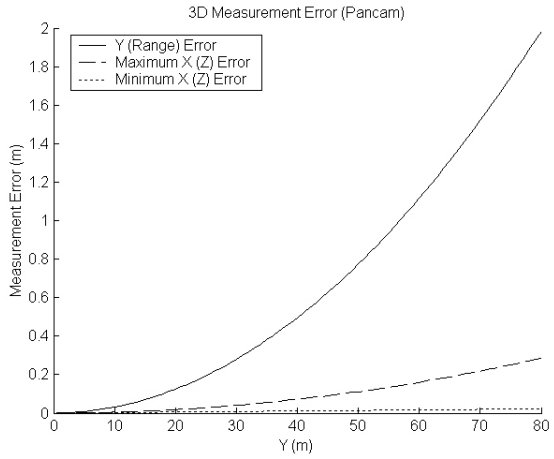

Figure 4. Expected 3D measurement errors for a Pancam stereo pair

3. TOPOGRAPHIC MAPPING CAPABILITY ANALYSIS OF A SINGLE-SITE PANORAMA

Both Spirit and Opportunity rovers took panoramas (360° or partial) and traversing stereo images at different positions (sites) along the traverse using Navcam and Pancam. The Pancam panoramas were acquired mainly at locations where substantial science explorations were needed; the Navcam panoramas were taken more frequently, at most of the sites. A typical 360° Navcam panorama consists of 10 stereo pairs (1 tier × 10 wedges) with an overlap of e.g., 20% among adjacent pairs. A complete three tier 360° Pancam panorama consists of 75 stereo pairs (3 tiers × 25 wedges) with a 10% overlap both in directions. Using these panoramas, we can produce local DTMs (digital terrain models) and orthophotos that cover an area of 60m × 60m (Navcam) or 120m × 120m (Pancam) with a resolution of 1cm per pixel. Figure 5 shows a typical orthophoto; it was automatically generated from the Navcam panorama taken by Spirit rover on Sol 100.

The mapping capability of a single-site panorama not only depends on the 3D measurement accuracy of stereo pairs (as analyzed above), but also depends on the accuracy and consistency of the pointing information of the adjacent stereo

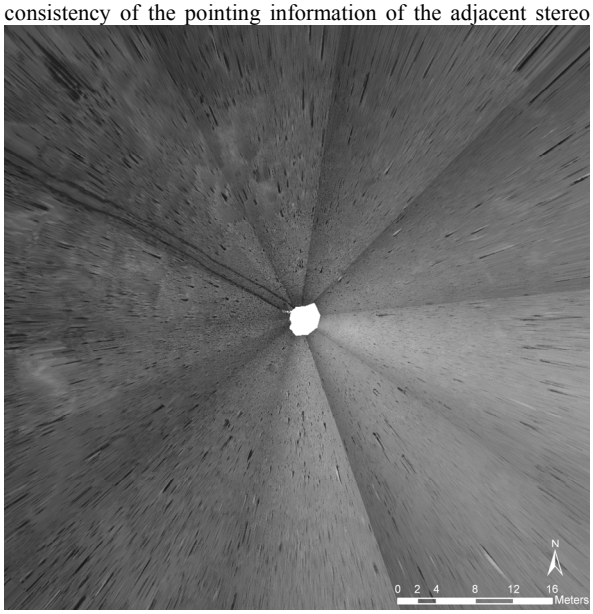

Figure 5. Orthophoto generated from Navcam images taken by Spirit on Sol 100 (60m × 60m, 1cm/pixel)

pairs within the panorama. The pointing information of the images is generally consistent within one panorama. It is stored in the CAHVOR (for original images) or CAHV (for linearized images) camera model in the telemetry data (Yakimovsky and Cunningham, 1978; Gennery, 2001). To give a theoretical estimation of the mapping errors at different locations for an orthophoto or DTM, we use a co-variance matrix to depict the position error. In a local (site) coordinate system whose X-axis points to north and Y-axis points to east, the (*X, Y*) position can be calculate from range *r* and azimuth θ using Equation 3 and its linearized form can be represented by Equation 4.

$$\begin{aligned} X &= r\cos\theta \\ Y &= r\sin\theta \end{aligned} \tag{3}$$

$$\begin{bmatrix} dX \\ dY \end{bmatrix} = \begin{bmatrix} \cos\theta & -r\sin\theta \\ \sin\theta & r\cos\theta \end{bmatrix} \begin{bmatrix} dr \\ d\theta \end{bmatrix} \tag{4}$$

Based on Equation 4 and the error propagation law, we can easily derive the position co-variance matrix as follows.

$$\begin{bmatrix} \sigma_X^2 & \sigma_{XY} \\ \sigma_{XY} & \sigma_Y^2 \end{bmatrix} = \begin{bmatrix} (\cos\theta)^2\sigma_r^2 + r^2(\sin\theta)^2\sigma_\theta^2 & (\sin\theta\cos\theta)\sigma_r^2 - r^2(\sin\theta\cos\theta)^2\sigma_\theta^2 \\ (\sin\theta\cos\theta)\sigma_r^2 - r^2(\sin\theta\cos\theta)^2\sigma_\theta^2 & (\sin\theta)^2\sigma_r^2 + r^2(\cos\theta)^2\sigma_\theta^2 \end{bmatrix} \tag{5}$$

Here, σ_r can be calculate from Equation 2a by substituting r for *Y*. During MER operations, we observed that the azimuthal inconsistency between adjacent stereo pairs (caused by telemetry error and other errors such as camera calibration error) was about one pixel and that it was reduced to within one pixel after bundle adjustment where additional constraint is implemented which requires the length of the fixed stereo camera baseline be the calibrated constant (Di et al., 2004). Thus, we assume an azimuthal error of one-pixel, i.e., $\sigma_\theta = \tan^{-1}(1 \text{ pixel}/f)$ in this analysis. Based on the co-variance matrix calculated from Equation 5, the error ellipses of a Navcam orthophoto are shown in Figure 6. It is apparent that the position errors are mainly in the radial directions and are consistent with the measurement accuracy shown in Figure 3. The error ellipses of a Pancam orthophoto can be calculated in the same way. For a DTM, the horizontal accuracy is generally the same as the corresponding orthophoto, and the elevation accuracy is in general higher than the horizontal accuracy as explained in Section 2.

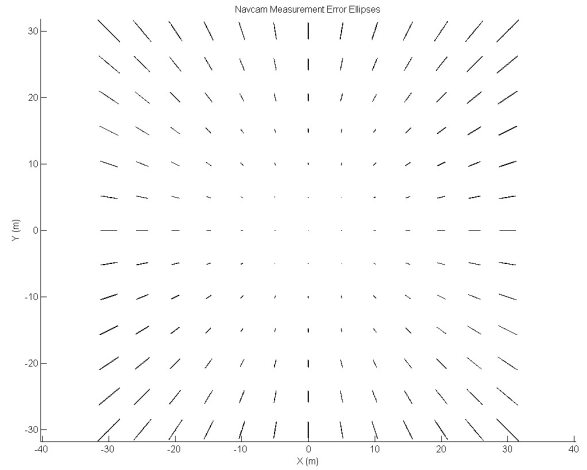

Figure 6. Error ellipses of positions in a Navcam orthophoto

In addition to the above theoretical analysis, the actual mapping accuracy of a single-site panorama can be estimated from data processing results. In the topographic mapping process, the CAHV models of the linearized images are converted to the conventional photogrammetric models (represented by interior and exterior orientation parameters) for 3D mapping (Di and Li, 2004). Then a bundle adjustment of the entire panorama is performed to refine the exterior orientation parameters to ensure that the DTM and orthophoto generated from bundle-adjusted images are of high accuracy and geometrically seamless. Therefore, the accuracies of the single-site DTM and orthophoto can be represented by the accuracy of the bundle adjustment of the panorama.

Since no absolute ground control is available on the Martian surface, the quality of the bundle adjustment is estimated by using discrepancies computed from adjacent image pairs where we have 2D image coordinates and 3D ground coordinates of the bundle-adjusted inter-stereo tie points (which link adjacent stereo pairs of the panorama (Xu, 2004). Specifically, the 3D accuracy is calculated from differences in the 3D ground coordinates of the inter-stereo tie points triangulated from different stereo pairs. The 2D accuracy is estimated using differences between the image coordinates in one image pair and those projected from the adjacent pairs. For example, for the Spirit panorama from Sol 100 (see Figure 5 for orthophoto), 62 inter-stereo tie points were automatically selected and used in the bundle adjustment. These tie points are within 30m of the camera, and thus can be measured reliably. Before adjustment, 2D accuracy was 1.43 pixels and 3D accuracy was 0.347m; after adjustment, 2D accuracy was 0.53 pixel and 3D accuracy was 0.344m. Both 2D and 3D accuracies were improved through the bundle adjustment; however, the improvement in 2D was more significant. The sub-pixel accuracy of the single-site panorama ensured the resultant orthophoto was geometrically seamless. The 3D accuracy at a certain range is generally consistent with the expected 3D measurement accuracy derived in Sections 2 and 3.

4. TOPOGRAPHIC MAPPING CAPABILITY ANALYSIS OF MULTI-SITE PANORAMAS ALONG THE ROVER TRAVERSE

In addition to individual DTMs and orthophotos generated at each rover position (site), we also produced a number of integrated DTMs using multi-site panoramas taken at different sites along the rover traverse. For example, starting Sol 576 and adding data sol by sol, we generated and expanded an integrated DTM for the Husband Hill summit area of the Spirit landing site using 3D ground points from multiple panoramas. The traverse segment lengths were 5m to 44m with most of the segments shorter than 18m. Recalling that the measurement error is expected to be less than 1m within a range of 27m for Navcam and 55m for Pancam, these traverse lengths help achieving the high quality of the ground points along the traverse. Figure 7 shows a 3D view of the integrated DTM of the Husband Hill summit area that was generated from multiple Navcam and Pancam panoramas from Sol 576 to Sol 609. This DTM covered an area of 230m × 180m with a 0.5m resolution. Contours with a 1m interval and the rover traverse are overlaid onto the DTM. The integrated DTM and the derived contour and slope maps were very useful in planning the rover traverse up to the summit of Husband Hill and down to the inner basin.

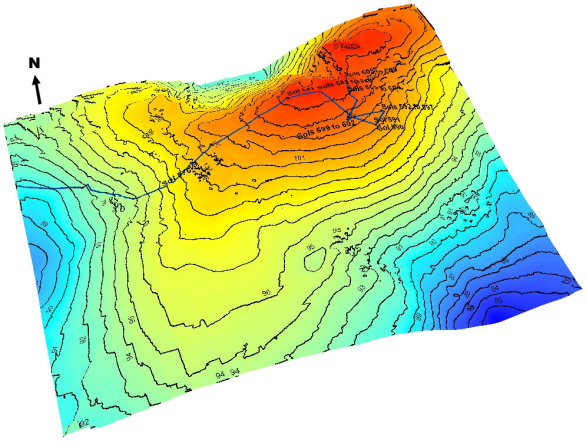

Figure 7. 3D view of the DTM, contour lines, and Spirit rover traverse at the top of Husband Hill

Similar to that for single-site panoramas, the accuracy of the integrated DTM generated from multiple panoramas depends on the 3D measurement accuracy of stereo pairs and the accuracy and consistency of the pointing information of the adjacent stereo pairs within one panorama. More importantly, the accuracy of the integrated DTM is heavily affected by the accuracy and consistency of the pointing information of images in different panoramas taken at different sites. In other words,

the mapping capability of multi-site panoramas is determined both by the mapping capability of single-site panoramas and the rover localization accuracy at each site. Due to wheel slippage, azimuthal angle drift, and other navigation errors, pointing information of images taken at adjacent sites (usually tens of meters apart) often has noticeable or significant inconsistencies. The incremental bundle adjustment, which is our key technology for rover localization and mapping in the MER mission operations, has been able to eliminate or reduce these inconsistencies, thus ensuring the accuracy of the integrated DTM. Therefore, the mapping capability of multi-site panoramas can be represented by the accuracy of the bundle adjustment of multiple panoramas along the traverse.

The bundle adjustment accuracy of multi-site panoramas is estimated by using discrepancies computed from 2D image coordinates and 3D ground coordinates of bundle-adjusted inter-stereo tie points and cross-site tie points (which link images between two adjacent sites (Xu, 2004). For most of the sites, the 2D accuracy after bundle adjustment is at a subpixel to one pixel level, and the 3D accuracy is at a centimeter to sub-meter level. These typical values represent the relative accuracy between two adjacent sites. However, mapping and localization error accumulates as the rover moves along its traverse. Since there is no absolute ground control on the Martian surface at this time, it is impossible to know the absolute accuracy of long-range rover localization and mapping in the MER mission. Below, we use geo-rectified MOC NA (Mars Orbiter Camera Narrow Angle) images as an independent data source to have a comparison.

As reported in Di et al. (2006), we compared the bundle-adjusted Spirit rover traverse with part of the actual rover track that can be seen on a 1m-resolution MOC NA image mosaic (Release No. MOC2-960) acquired and processed by Malin Space Science Systems (Malin, 2005). The difference between the two rover tracks at the last point (Spirit's Sol 183) was 12m (about 0.4% of the 3081m distance traveled from the lander). We also compared the bundle-adjusted location of Spirit rover on Sol 562 with a MOC NA image taken at Spirit's Sol 652 in which the rover itself can be identified. A difference was found of about 20m, or 0.4% of the 4559m overall traverse from the lander. These differences consist of the georeferencing error of the multi-strip MOC base map along with the residuals of the bundle adjustment..

5. TOPOGRAPHIC MAPPING CAPABILITY ANALYSIS OF WIDE-BASELINE STEREO IMAGES

In single-site or multi-site mapping, the 3D ground points were calculated from Navcam or Pancam stereo images that were acquired by left and right cameras separated by a "hard" baseline. Due to the ranging limitations of hard baseline stereo images (see Figures 3 and 4), wide-baseline stereo images were acquired at some locations in order to map far-range terrain for planning long term rover traverses. A wide-baseline stereo pair is formed by two or more images taken at two rover positions with a "soft" baseline that is much wider that the "hard" baseline. For example, at Home Plate of the Spirit landing site, in order to map the up-slope terrain of McCool Hill, wide-baseline images were taken using Pancam at two sites about 8m apart: Site APFI (on Sols 774 and 775) and Site APGB (on Sols 776 to 778). The images include 2-tier × 8-wedge Pancam red (stereo) and blue (single) images from both sites. Figure 8 is a mosaic of the images taken at Site APFI showing McCool Hill, whose summit is about 400m from the rover. Wide-baseline stereo pairs were established by a single image of Site APFI and another single image that had sufficient overlap from Site APGB. The 3D ground points were calculated from matched homologous points from wide-baseline stereo pairs using the bundle-adjusted exterior orientation parameters. A 1m-resolution DTM was generated by using 24,262 ground points. A half-meter-interval contour map was then derived from the DTM; it is shown in Figure 9, in which the important terrain features (labeled with names) can be clearly identified. Figure 10 shows a 3D view of the wide-baseline DTM of McCool Hill.

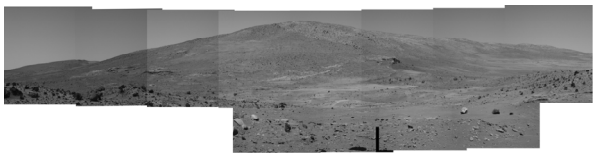

Figure 8. Mosaic of Pancam images for wide-baseline mapping of McCool Hill

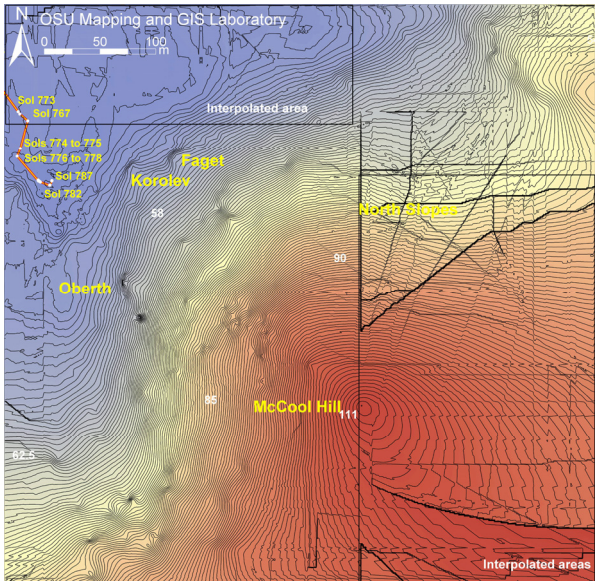

Figure 9. DTM and contour map of McCool Hill

The mapping accuracy of the wide-baseline images is reflected by the accuracy of the bundle adjustment of the two sites. All the stereo and single images at both sites were used in this bundle adjustment. Using 74 inter-stereo and cross-site tie points as check points, the accuracy was found to be 1.2 pixels in 2D and 0.87m in 3D after bundle adjustment; the bundle adjusted baseline was 7.70m. As a result, wide-baseline mapping significantly improved the mapping capability of rover stereo images from tens of meters to up to 400 meters. The successful employment of wide-baseline mapping technology enabled ground image-based long-term planning as well as scientific investigations of large terrain features (e.g., the 156m-diameter Endurance Crater at the Opportunity landing site). It should be emphasized that the bundle adjustment is critical in wide-baseline mapping, because the baseline and relative orientations between the left and right images of a wide-baseline stereo pair are not as fixed as those of the "hard" baseline stereo pairs and thus must be fine-tuned by the bundle adjustment to achieve a high level of accuracy.

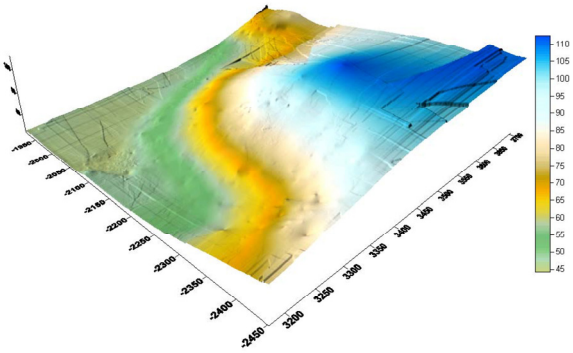

Figure 10. 3D view of the DTM of McCool Hill

6. CONCLUSIONS

This paper presents a relatively comprehensive analysis of the topographic mapping capabilities of the MER Navcam and Pancam images. The expected measurement error is less than 1m within a range of 27m for Navcam stereo pairs and 55m for Pancam stereo pairs. After bundle adjustment, a single-site panorama was found to have a centimeter to sub-meter mapping accuracy within an area of 60m × 60m (Navcam) or 120m × 120m (Pancam). The bundle-adjusted multi-site panoramas have a difference of 0.4% of the accumulated length of the rover traverse compared wit orbital images. Wide-baseline mapping with bundle adjustment has been found to significantly improve the mapping capability of the rover images. An example from the Spirit landing site has demonstrated that wide-baseline Pancam images with an 8m baseline can map far-range terrain (up to 400m) with sub-meter accuracy. We hope this analysis is helpful for understanding the attainable accuracies of the MER rover images and for best usage of the mapping products during and after the MER mission. These accuracy analysis methods can also be used to evaluate the topographic mapping capabilities of the imaging sensors of future Mars landed missions.

ACKNOWLEDGEMENTS

Funding of this research by the Mars Exploration Program of NASA is acknowledged.

REFERENCES

Alexander, D.A, Deen, R.G., Andres, P.M., Zamani, P., Mortensen, H.B., Chen, A.C., Cayanan, M.K., Hall, J.R., Klochko, V.S., Pariser, O., Stanley, C.L., Thompson, C.K., and Yagi, G.M., 2006. Processing of Mars Exploration Rover imagery for science and operations planning, *Journal of Geophysical Research-Planets*, 111, pp. E02S02 (doi:10.1029/2005JE002462).

Arvidson, R.E., Anderson, R.C., Bartlett, P., Bell, J.F. III, Blaney, D., Christensen, P.R., Chu, P., Crumpler, L., Davis, K., Ehlmann, B.L., Fergason, R., Golombek, M.P., Gorevan, S., Grant, J.A., Greeley, R., Guinness, E.A., Haldemann, A.F.C., Herkenhoff, K., Johnson, J., Landis, G., Li, R., Lindemann, R., McSween, H., Ming, D.W., Myrick, T., Richter, L., Seelos, F.P. IV, Squyres, S.W., Sullivan R.J., Wang, A., Wilson, J., 2004. Localization and physical properties experiments conducted by Spirit at Gusev Crater. *Science*, Special Issue on MER 2003 Mission, 305(5685), pp. 821-824.

Bell, J.F. III, Squyres, S.W., Herkenhoff, K.E., Maki, J.N., Arneson, H.M., Brown, D., Collins, S.A., Dingizian, A., Elliot, S.T., Hagerott, E.C., Hayes, A.G., Johnson, M.J., Johnson, J.R., Joseph, J., Kinch, K., Lemmon, M.T., Morris, R.V., Scherr, L., Schwochert, M., Shepard, M.K., Smith, G.H., Sohl-Dickstein, J.N., Sullivan, R.J., Sullivan, W.T., Wadsworth, M., 2003. Mars exploration rover Athena panoramic camera (Pancam) investigation. *Journal of Geophysical Research-Planets*, 108(E12), pp. 8063 (doi:10.1029/2003JE002070).

Di, K., and Li, R., 2004. CAHVOR camera model and its photogrammetric conversion for planetary applications. *Journal of Geophysical Research-Planets*, 109(E4), pp. E04004 (doi:10.1029/2003JE002199).

Di, K., Xu, F., and Li, R., 2004. Constrained bundle adjustment of panoramic stereo images for Mars landing site mapping. The 4th International Symposium on Mobile Mapping Technology (MMT2004), Kunming, China, March 29-31, 2004 (CD-ROM).

Di, K., Xu, F., Wang, J., Niu, X., Serafy, C., Zhou, F. Li, R., and Matthies, L.H., 2005. Surface imagery based mapping and rover localization for the 2003 Mars exploration rover mission. *Proceeding of ASPRS 2005 Annual Conference*, Baltimore, MD, March 7-11, 2005 (CD-ROM).

Di, K., Wang, J., Agarwal, S., Brodyagina, E., Yan, L., Li, R. and Matthies, L.H., 2006. New photogrammetric techniques used in the 2003 Mars exploration rover mission. *Proceeding of ASPRS 2006 Annual Conference*, Reno, Nevada, May 1-5, 2006 (CD-ROM).

Gennery, D.B., 2001. Least-squares camera calibration including lens distortion and automatic editing of calibration points. In: *Calibration and Orientation of Cameras in Computer Vision*, A. Gruen and T.S. Huang, Editors, Springer-Verlag, New York, pp. 123-136.

Li, R., Di, K., Matthies, L.H., Arvidson, R.E., Folkner, W.M., and Archinal, B.A., 2004. Rover localization and landing site mapping technology for 2003 Mars Exploration Rover mission. *Photogrammetric Engineering & Remote Sensing*, 70(1), pp. 77-90.

Li, R., Squyres, S.W., Arvidson, R.E., Archinal, B.A., Bell, J.F. III, Cheng, Y., Crumpler, L., Des Marais, D.J., Di, K., Ely, T.A., Golombek, M., Graat, E., Grant, J., Guinn, J., Johnson, A., Greeley, R., Kirk, R.L., Maimone, M., Matthies, L. H., Malin, M., Parker, T., Sims, M., Soderblom, L.A., Thompson, S., Wang, J., Whelley, P., Xu, F., 2005. Initial results of rover localization and topographic mapping for the 2003 Mars Exploration Rover Mission. *Photogrammetric Engineering and Remote Sensing*, 71(10), pp. 1129-1142.

Li, R., Archinal, B.A., Arvidson, R.E., Bell, J.F. III, Christensen, P., Crumpler, L., Des Marais, D.J., Di, K., Duxbury, T., Golombek, M., Grant, J., Greeley, R., Guinn, J., Johnson, A., Kirk, R.L., Maimone, M., Matthies, L.H., Malin, M., Parker, T., Sims, M., Thompson, S., Squyres, S.W., Soderblom, L.A., 2006. Spirit rover localization and topographic mapping at the landing site of Gusev crater, Mars. *Journal of Geophysical Research-Planets*, 111, pp. E02S06 (doi:10.1029/2005JE002483).

Maki, J.N., Bell, J.F. III, Herkenhoff, K.E., Squyres, S.W., Kiely, A., Klimesh, M., Schwochert, M., Litwin, T., Willson, R., Johnson, A., Maimone, M., Baumgartner, E., Collins, A., Wadsworth, M., Elliot, S. T., Dingizian, A., Brown, D., Hagerott, E. C., Scherr, L., Deen, R., Alexander, D., Lorre, J., 2003. Mars exploration rover engineering cameras. *Journal of Geophysical Research-Planets*, 108(E12), 8071, pp. 12-1 to 12-24 (doi:10.1029/2003JE002077).

Malin, M., 2005. MGS MOC Images of Mars Exploration Rover Landing Sites, Malin Space Science Systems, San Diego, CA. http://www.msss.com/mer_mission/index.html (accessed 1 Mar. 2007).

Squyres, S.W., Arvidson, R.E., Baumgartner, E.T., Bell, J.F. III, Christensen, P.R., Gorevan, S., Herkenhoff, K.E., Klingelhöfer, G., Madsen, M.B., Morris, R.V., Rieder, R., Romero, R.A., 2003. Athena Mars rover science investigation. *Journal of Geophysical Research-Planets*, 108(E12), pp. 8062 (doi:10.1029/2003JE002121).

Squyres, S.W., Arvidson, R.E., Bell, J.F. III, Brückner, J., Cabrol, N.A., Calvin, W., Carr, M.H., Christensen, P.R., Clark, B.C., Crumpler, L., Des Marais, D.J., d'Uston, C., Economou, T., Farmer, J., Farrand, W., Folkner, W., Golombek, M., Gorevan, S., Grant, J.A., Greeley, R., Grotzinger, J., Haskin, L., Herkenhoff, K.E., Hviid, S., Johnson, J., Klingelhöfer, G., Knoll, A., Landis, G., Lemmon, M., Li, R., Madsen, M.B., Malin, M.C., McLennan, S.M., McSween, H.Y., Ming, D. W., Moersch, J., Morris, R.V., Parker, T., Rice, J.W. Jr., Richter, L., Rieder, R., Sims, M., Smith, M., Smith, P., Soderblom, L.A., Sullivan, R., Wänke, H., Wdowiak, T., Wolff, M., Yen, A., 2004. The Spirit rover's Athena science investigation at Gusev Crater, Mars. *Science*, Special Issue on MER 2003 Mission, 305(5685), pp. 794-799.

Wang, Z., 1990. *Principles of photogrammetry (with remote sensing)*. Publishing House of Surveying and Mapping, Beijing, China, 366 p.

Xu, F., 2004. Mapping and localization for extraterrestrial robotic explorations. Ph. D. Dissertation, The Ohio State University, Columbus, OH.

Xu, F., Di, K., Wang, J., and Li, R., 2005. Techniques of registration and mapping in Mars exploration rover (MER) 2003 mission. *Proceeding of ASPRS 2005 Annual Conference, Baltimore, Maryland*, March 7-11, 2005 (CD-ROM).

Yakimovsky, Y., and Cunningham, R., 1978. A System for Extracting Three-dimensional Measurements from a Stereo Pair of TV Cameras. *Computer Graphics and Image Processing*, 7, pp. 195-210.

Zhang Z., and Zhang J., 1997. *Digital photogrammetry*. Press of Wuhan Technical University of Surveying and Mapping, Wuhan, China, pp. 171-172 (in Chinese).